JOURNAL OF GEOPHYSICAL RESEARCH, VOL. 105, NO. A2, PAGES 2325–2335, FEBRUARY 1, 2000

Multisatellite observations of large magnetic depressions in the solar wind

G. Chisham,[1] S. J. Schwartz, D. Burgess, and S. D. Bale[2]

Astronomy Unit, Queen Mary and Westfield College, London, England, United Kingdom

M. W. Dunlop

Space and Atmospheric Physics Group, Imperial College, London, England, United Kingdom

C. T. Russell

Institute of Geophysics and Planetary Physics, University of California, Los Angeles

Abstract. Two large depressions in the magnitude of the interplanetary magnetic field, lasting ~10–20 min, have been observed in the solar wind just upstream of the Earth's bow shock by three spacecraft (Active Magnetospheric Particle Tracer Explorer UK Subsatellite (AMPTE UKS), AMPTE Ion Release Module (IRM), and ISEE 1). The multiple satellite observations show that the depressions are convecting with the ambient solar wind. Analysis of the depression boundaries shows that they are tangential discontinuities with normals aligned approximately parallel to the GSE x direction. The electron distributions measured within the structures are remarkably isotropic when compared to the more anisotropic distributions found in the ambient solar wind. There is also a reduction in plasma wave activity during the depressions. The depressions exhibit characteristics similar to those of solar wind magnetic holes but are much larger than has been typically observed. The depressions also display similarities with encounters of the heliospheric plasma sheet and heat flux dropouts, both of which are typically observed near sector boundaries, close to the heliospheric current sheet. The nature of these depressions is discussed in the context of magnetic hole and heliospheric plasma sheet observations. A large magnetic hole structure formed from a conglomeration of small holes appears the more likely scenario for the observed depressions.

1. Introduction

There are several interplanetary phenomena that are characterized by reductions in the magnitude of the interplanetary magnetic field (IMF). Many of these phenomena are thought to be associated with interplanetary current sheets, particularly the heliospheric current sheet (HCS). "Magnetic holes" [e.g., *Burlaga*, 1968], "heat flux dropouts" (HFDs) [*McComas et al.*, 1989], and "planar magnetic structures" (PMSs) [e.g., *Nakagawa et al.*, 1989] all display reductions in magnetic field intensity and have at some time been associated with crossings (or partial crossings) of the HCS at IMF sector boundaries or interactions with the surrounding heliospheric plasma sheet (HPS) [e.g., *Crooker et al.*, 1996a,b]. Magnetic holes have also been observed by the Ulysses spacecraft at high heliolatitudes, far from the HCS [*Winterhalter et al.*, 1994b], where they are thought to grow out of the mirror instability. Closer to the Earth there are structures called "hot flow anomalies" (HFAs) [e.g., *Schwartz et al.*, 1985; *Thomsen et al.*, 1986] which display reductions in magnetic field intensity flanked by regions of compressed, shocked solar wind. They are generally thought to be associated with interactions between interplanetary current sheets and the Earth's bow shock [see *Schwartz*, 1995, and references therein]. These varied observations of different phenomena displaying reductions in magnetic field strength have some similarities and may in some cases describe similar physical processes. However, the origins of many of these phenomena are still uncertain.

The HCS represents the boundary between the generally antisunward IMF related to the dominant po-

[1]Now at British Antarctic Survey, Natural Environment Research Council, Cambridge, England, United Knigdom.

[2]Now at Space Sciences Laboratory, University of California, Berkeley.

Paper number 1999JA900446.
0148-0227/00/1999JA900446$09.00

larity in one solar hemisphere and the generally sunward IMF related to the other solar hemisphere. It is typically ~3000-10,000 km thick [*Winterhalter et al.*, 1994a] and is surrounded by the HPS, which is ~20-30 times thicker. The HPS is characterized by reductions in the magnitude of the IMF [e.g., *Behannon et al.*, 1981] and by enhanced density and hence enhanced plasma β. The structure of the HPS/HCS system is complex, often consisting of a number of large-angle, directional discontinuities (mainly tangential discontinuities) occurring on different timescales. The precise scale and variability of the HPS are uncertain. It is also not clear to what extent the HPS is static and convected or dynamic and wavelike, or whether it typically contains several current sheets [e.g., *Crooker et al.*, 1996a]. Multiple traversals of the HCS are often observed [e.g., *Behannon et al.*, 1981] although it is not clear how much these variations represent internal spatial structure or local fluctuations in the position of the sheet.

Observations of the HPS have also been associated with observations of HFDs and PMSs, both of which display reductions in magnetic field intensity [*Crooker et al.*, 1996a,b]. HFDs [e.g., *McComas et al.*, 1989] are intervals when the flow of antisunward, suprathermal electrons decreases suddenly, leaving a nearly isotropic velocity distribution. HFDs are typically accompanied by reductions in magnetic field intensity and increases in density. The origin of HFDs is uncertain; they are possibly signatures of flux tube disconnection from the Sun [*McComas et al.*, 1989], a result of enhanced Coulomb scattering of halo electrons in transit from the Sun to the Earth [*Fitzenreiter and Ogilvie*, 1992], or a result of mechanisms involving wave particle interactions [*Crooker et al.*, 1996b]. PMSs [e.g., *Nakagawa et al.*, 1989; *Farrugia et al.*, 1990] are distinctive features in the solar wind characterized by a series of abrupt changes in the IMF direction with the field remaining parallel to a single plane. The large changes in the field direction (generally tangential discontinuities) are often accompanied by clear field depressions. Again, their origin is uncertain; it has been suggested that these structures represent magnetic islands resulting from reconnection in solar magnetic tongues [*Nakagawa et al.*, 1989] or that they represent a series of intertwined flux ropes/plasma sheets close to the HCS [*Crooker et al.*, 1996a,b].

Magnetic holes have been observed in the solar wind for 30 years [e.g., *Burlaga*, 1968; *Turner et al.*, 1977; *Dobrowolny et al.*, 1979; *Winterhalter et al.*, 1994b]. They were originally defined as temporary reductions in the IMF magnitude to less than 1 nT [*Turner et al.*, 1977] although this definition was based solely on observations of magnetic holes at 1 AU. The majority of the observations described holes bounded by discontinuities, characterized by both a dip in B and a change in field direction. An early statistical study of magnetic holes by *Klein and Burlaga* [1980] showed that the number of magnetic holes that occurred near IMF sector boundaries was 3 times greater than that observed in the average solar wind environment. Many of these events often displayed large rotations of the IMF direction (~100°-200°), suggesting that they represented encounters with the HPS/HCS. More recently, *Winterhalter et al.* [1994b] defined magnetic holes as a dip in the IMF magnitude such that $B_{\min}/B_0 \leq 0.5$, where $B_{\min}$ was the minimum magnetic field magnitude observed and B_0 was the average ambient magnetic field strength. They observed a number of holes, termed "linear" magnetic holes, which appeared to show very little change in field direction (<20°). Many of these events were observed away from the ecliptic plane and hence were unlikely to be associated with the HPS/HCS. Previous studies have suggested that typical magnetic holes have a temporal extent ~2-130 s (with an approximate average of 50 s) [*Turner et al.*, 1977], which suggests a spatial extent ~200 R_L (ion Larmor radii) assuming convection with the solar wind. Data search techniques in these studies have generally precluded the observation of larger magnetic holes.

Recent studies [e.g., *Winterhalter et al.*, 1994b] have attempted to obtain a multi-instrument perspective of magnetic holes. Correlations have been reported between the occurrence of magnetic holes and a range of plasma waves; *MacDowall et al.* [1996] and *Lin et al.* [1995] have shown that Langmuir waves are a common feature of magnetic holes. Lin et al. also showed that ion acoustic and whistler mode waves can occur in magnetic holes and that for holes bounded by directional discontinuities, plasma waves are often a feature of the hole edges. The frequent detection of these waves in magnetic holes suggests that they are not static structures but are continually evolving. Despite many observations describing magnetic hole characteristics, their origin and stability have not been clearly determined. *Tsurutani et al.* [1992] and *Winterhalter et al.* [1994b] have suggested that magnetic holes are evolving mirror mode structures convecting with the solar wind. *Pantellini* [1998] has developed this idea, showing how magnetic holes can grow out of the nonlinear mirror instability.

Despite the number of observations of magnetic holes, interactions with the HPS/HCS, and other structures displaying sizeable reductions in the intensity of the IMF, there is still confusion regarding the definition of these structures. It is likely that these observations relate to more than one phenomenon and in particular there appear to be two classes of magnetic holes, one associated with the HPS/HCS and another that grows out of the mirror instability. There is still uncertainty regarding the size of magnetic holes (their observed duration), their location with respect to the HPS/HCS, and the extent of their associated magnetic field rotations. Recently, *Lin et al.* [1995] presented observations of a "shallow" hole ($\Delta B/B_0$ ~0.5) with a duration of ~45 min bounded by rotational discontinuities. Their observation described a much larger structure than the

typically observed magnetic hole. The previously observed typical size of magnetic holes may be a result of the selection criteria employed; *Winterhalter et al.* [1994b] only identified magnetic field reductions within a 300 s sliding window and hence had a maximum event duration of 150 s.

In this paper we present observations of two large depressions in the IMF (i.e., B dipped to ~1 nT), which occurred on November 26, 1984, upstream of the bow shock (these depressions were first reported by *Chisham et al.* [1997]). These structures exhibited similarities to both magnetic holes and HPS encounters but had much sharper boundaries than those generally observed. We present particle, wave, and magnetic field data describing these events from three spacecraft (Active Magnetospheric Particle Tracer Explorer UK Subsatellite (AMPTE UKS), AMPTE Ion Release Module (IRM), and ISEE 1) and attempt to unravel the characteristics of the depressions and compare them with other solar wind observations of large magnetic field reductions. Although the AMPTE UKS data set shows no other large depressions of this nature, present studies using the Ulysses data set (M. Fränz, personal communication, 1999) show that they are not uncommon features of the IMF, even at high heliolatitudes.

2. Event Overview

The depressions in the IMF that occurred on November 26, 1984, were observed by three satellites in the solar wind; AMPTE UKS and AMPTE IRM were located just outside the bow shock whereas ISEE 1 was farther upstream. Figure 1 displays the positions of these three spacecraft projected into the GSE x-y plane (the displacement of the spacecraft in the GSE z direction is minimal).

Figure 2 displays the magnetic field magnitude from the two AMPTE spacecraft [*Southwood et al.*, 1985; *Lühr et al.*, 1985] and ISEE 1 [*Russell*, 1978] for an extended time interval to illustrate the solar wind environment before, during, and after the events (some data gaps are apparent within the ISEE 1 and at the end of the AMPTE UKS data). The section of data which contains the magnetic depressions is highlighted by two dashed lines (at 0800 and 0930 UT). Before this interval the spacecraft were located within the ion foreshock owing to the direction of the IMF. At ~0715 UT the ambient field direction changed suddenly, moving the spacecraft into unconnected solar wind. In the following couple of hours two large depressions in the IMF were observed within which the field magnitude dropped to ~1 nT. Only one of the depressions is apparent in the ISEE 1 observations owing to a data gap. In the AMPTE data this time interval was also interspersed with small bursts of ULF waves, a result of small changes in the field direction placing the spacecraft temporarily in the foreshock region. These bursts were not seen at ISEE 1, owing to its position farther upstream from the bow shock. After the time interval containing the depressions the AMPTE satellites passed through the bow shock and into the magnetosheath at ~1030 UT.

Figure 3 displays multi-instrument data from the AMPTE UKS magnetic field experiment [*Southwood et al.*, 1985], the AMPTE UKS ion experiment [*Coates et al.*, 1985], and the AMPTE UKS electron experiment [*Shah et al.*, 1985] at 10 s resolution for the time interval between 0800 and 0930 UT.

Figure 3a displays the magnetic field magnitude for the interval. The two large depressions in the IMF magnitude are very clear at ~0813–0819 UT and 0900–0918 UT. During these intervals the field magnitude drops sharply from ~5 to ~1-2 nT ($\Delta B/B_0$ ~0.7, where B_0 represents the ambient solar wind magnetic field strength). Figure 3b displays the magnetic field orientation in GSE colatitude θ_B and GSE longitude ϕ_B. It is clear that coincident with the large drops in field magnitude which define the depressions there is only a small change in the field direction (~30°–60°). The field direction does display a larger change within the second depression which results in AMPTE UKS being temporarily within the ion foreshock region. Field-aligned ion beams consistent with AMPTE UKS being located in the outer ion foreshock are observed (not shown) be-

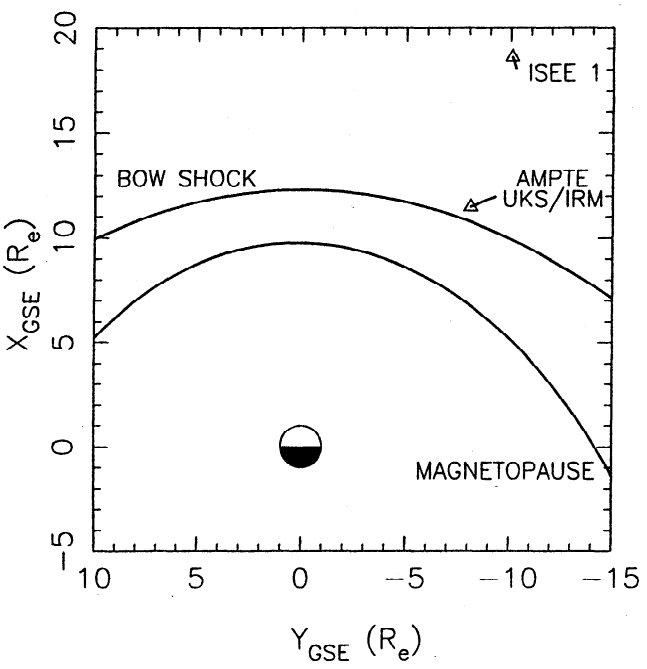

Figure 1. The positions of AMPTE UKS, AMPTE IRM and ISEE 1 at the time of the event projected into the GSE x-y plane. The solid lines represent the path of the spacecraft between 0800 and 0930 UT. The symbol at the end of each line represents its position at 0930 UT. The paths of AMPTE UKS and AMPTE IRM are almost identical and have therefore been presented as one line. Also shown are estimates of the bow shock and magnetopause positions scaled from a bow shock crossing by AMPTE IRM at 1030 UT.

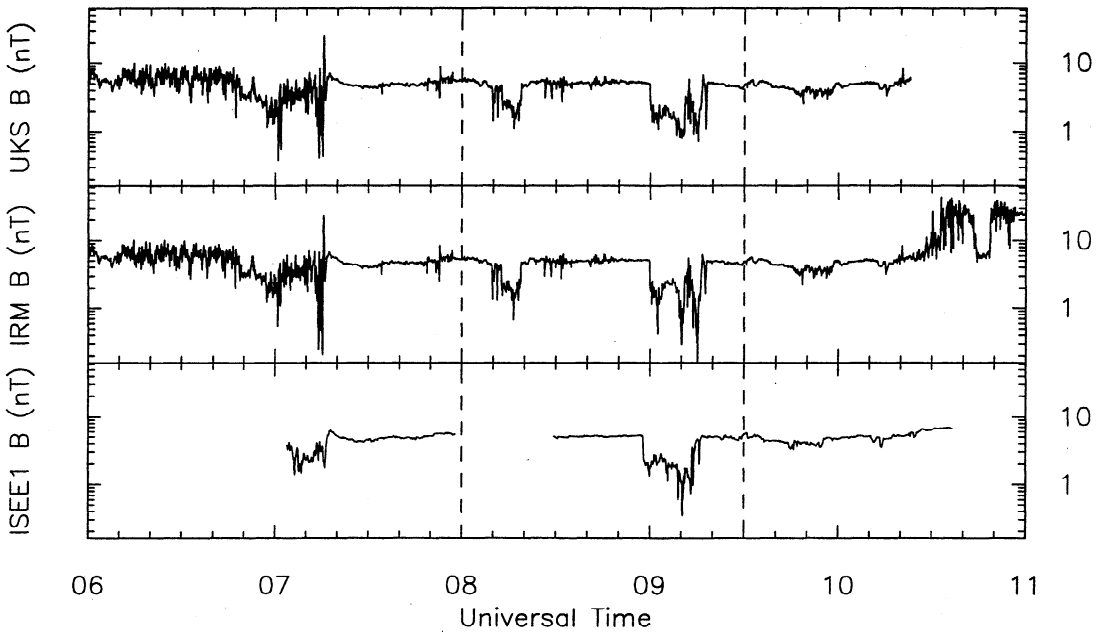

Figure 2. The magnetic field magnitude measured by AMPTE UKS, AMPTE IRM, and ISEE 1 before, during, and after the event. The main interval of interest containing the magnetic depressions is between the dashed lines.

tween ~0910 and 0915 UT. ISEE 1, farther upstream than AMPTE UKS, shows no evidence of entering the ion foreshock.

Figure 3c shows the ion density during the interval. Although noisy, the ion density clearly increases within both depressions; the average ion density within the depressions (excluding the fluctuations caused by entry into the foreshock) is ~ 1.2 times that in the ambient solar wind. Figure 3d displays the magnitude of the bulk solar wind velocity calculated from the ion distributions. Apart from a few fluctuations associated with excursions into the foreshock regions, the solar wind velocity magnitude varies little, being ~370-380 km s^{-1}.

Figure 3e displays the ion and electron temperature variations. Both the ion and electron distributions show no significant change in temperature between the ambient solar wind and the depressions. However, high-resolution electron data reveal subtle changes in the electron distribution and temperature between the ambient solar wind and the depressions. The availability of two-dimensional electron distributions allows the separate calculation of the electron temperatures parallel and perpendicular to the background magnetic field direction and hence an electron temperature anisotropy ($A_e \equiv T_{e\perp}/T_{e\parallel}$), which is displayed in Figure 3f. For most of the interval an anisotropy exists in the electron data ($A_e < 1$; $T_{e\parallel} > T_{e\perp}$), which is typical of solar wind electron distributions [e.g., *Phillips et al.*, 1989, and references therein]. However, during the magnetic depressions, $A_e \sim 1$ (i.e., the electron distributions are approximately isotropic). This feature of the electron distributions is addressed in more detail in section 3.

Figure 3g displays the electron and ion β for the interval. As would be expected, owing to the large drop in the magnetic field magnitude, β is extremely large (> 10) during the magnetic depressions and ~1 elsewhere.

It was not possible to reliably confirm if a total pressure balance existed between the magnetic depressions and the ambient solar wind. Estimates of the total pressure variation showed an approximate 25% drop in total pressure within the depressions. There were no apparent dynamic processes at work which would imply that the depressions were shrinking rapidly, and hence we are forced to conclude that the deficit is related to the inadequacy of the AMPTE UKS data. Firstly, we had no measure of the ion temperature anisotropy, and so no estimate of the perpendicular ion temperature could be made. Secondly, the size of the uncertainty in the density measurements was unknown; indeed, high-resolution plasma wave data suggested that the density was ~12 cm^{-3} (R.R. Anderson, personal communication, 1999), ~50% higher than that estimated from the distribution functions. Thirdly, no reliable measurements of the α particle variations or the suprathermal ion populations could be made. These shortcomings made an accurate quantitative analysis of the plasma pressure variations very difficult.

3. Electron Observations

High-resolution electron data from AMPTE UKS have allowed a detailed comparison to be made between the electron distribution measured within the magnetic

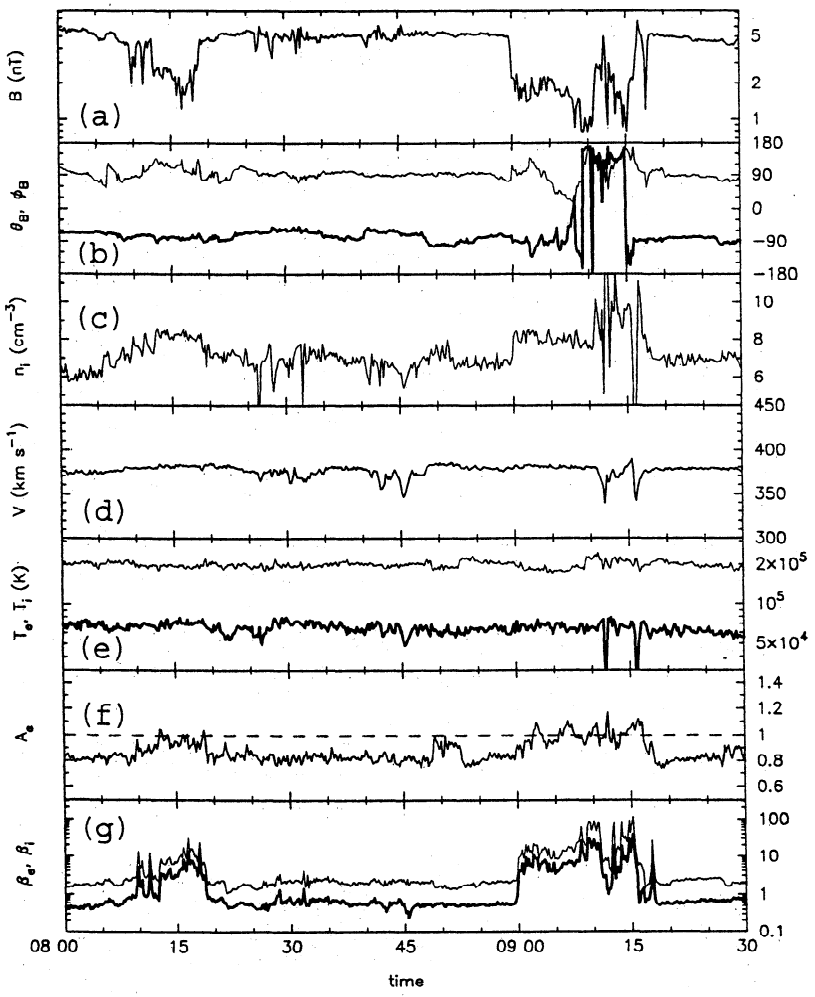

Figure 3. AMPTE UKS magnetic field, and ion and electron moments at 10 s resolution. (a) Magnetic field magnitude. (b) Magnetic field direction, including GSE colatitude (θ_B) (thin line) and GSE longitude (ϕ_B) (thick line). (c) Ion denisty. (d) Solar wind velocity. (e) Electron (thin line) and ion (thick line) temperatures. (f) Electron temperature anisotropy ($T_\perp/T_\parallel$). (g) Electron (thin line) and ion (thick line) β.

depressions and that measured in the ambient solar wind. Instrumental details of the AMPTE UKS electron instrument and data reduction methods used in the estimation of the distribution functions can be found in the work of *Shah et al.* [1985] and *Chisham et al.* [1996]. Figure 4a presents two-dimensional electron distributions in parallel-perpendicular velocity space representing the second depression and the ambient solar wind just prior to this depression. Six contours of each distribution function are presented each separated by a decade of phase space density. The data have been binned into 20 separate pitch angle bins illustrated by the triangle symbols which are equally spaced in $\cos\alpha$, where α represents pitch angle. Figures 4b and 4c present parallel and perpendicular cuts through the depression and the ambient solar wind distributions, respectively. The electron distributions in Figure 4 are collected over 5 min which results in statistically reliable estimates of the respective distributions.

A comparison of the two-dimensional distributions presented in Figure 4a shows that the ambient solar wind distribution, parallel and antiparallel to the magnetic field direction, is somewhat hotter than the depression distribution. The surplus in the parallel direction represents the solar wind heat flux which is absent in the depression. Comparison of the cuts of the two distributions reveals that the electron distributions are very isotropic within the depressions (Figure 4b), whereas those in the ambient solar wind (Figure 4c) show an anisotropy ($T_\parallel > T_\perp$) which is predominantly a result of the solar wind heat flux. These differences are manifest in the electron temperature anisotropy displayed in Figure 3.

Although electron distributions in the solar wind are generally anisotropic, isotropic distributions are not uncommon and can occur for a number of reasons. Mapping the solar wind electron distribution from the ambient solar wind into the depression assuming conser-

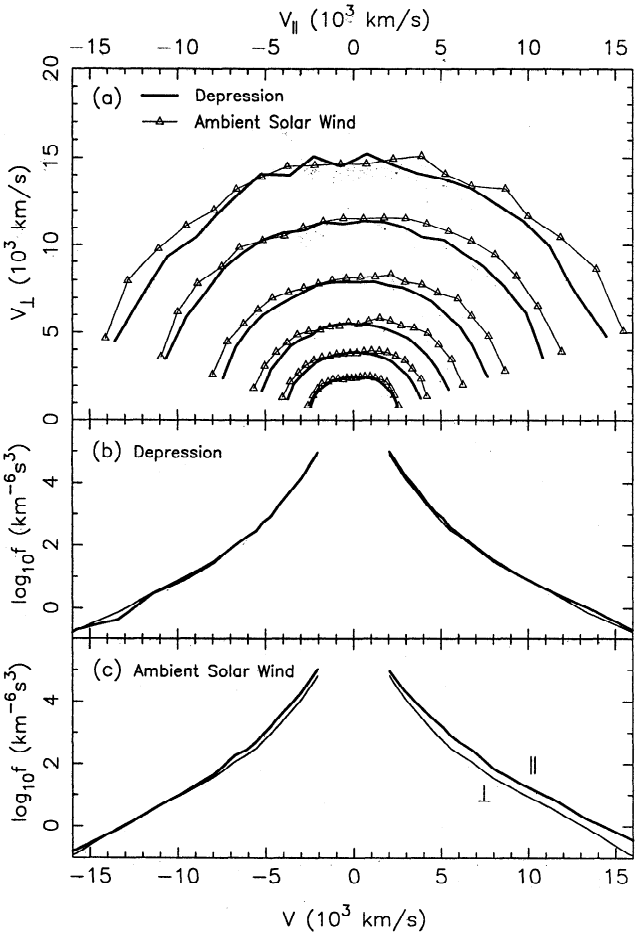

Figure 4. (a) Two-dimensional electron distributions (in parallel-perpendicular velocity space) representing the ambient solar wind (0855–0900 UT) and the second depression (0900–0905 UT). (b) Parallel (bold line) and perpendicular (thin line) cuts through the depression distribution. (c) Parallel (bold line) and perpendicular (thin line) cuts through the ambient solar wind distribution.

vation of total energy and magnetic moment predicts a more anisotropic distribution in the lower field region [e.g., *Chisham et al.*, 1996], contrary to the observations shown in Figure 4. Therefore the adiabatic response of electrons moving between the two regions could not produce the isotropic distributions observed here. Moreover, we show later that the depression boundaries are tangential discontinuities, so there is no magnetic connection between the two regions, and any Liouville mapping is inappropriate. Figure 4a suggests that the isotropy in the depression is associated mainly with a loss of the solar wind electron heat flux.

4. Plasma Wave Observations

Isotropic electron distributions can also occur as a result of wave particle scattering. Figure 5 presents plasma wave data from the AMPTE IRM plasma wave experiment [*Häusler et al.*, 1985] for the interval 0800 - 0930 UT which shows the wave activity during the depressions. The ELF/MF spectrum analyzer on AMPTE IRM measured wave power in 16 channels which were equally spaced in log (frequency) from 31 Hz to 178 kHz and are presented in Figure 5 at 5 s resolution; the darker shading represents the higher intensity levels.

In Figure 5, wave activity is evident during most of the interval presented, mainly Langmuir and beam mode waves associated with the electron foreshock region [c.g., *Gurnett*, 1985]. However, there seems to be no increase in wave activity within the depressions; in fact, a drop in wave activity is more apparent, especially during the second depression. The reduction in wave activity observed may be a result of the isotropization of the electron distribution (i.e., the loss of a source of free energy). Although there is no significant wave activity present in the depressions, this does not rule out the possibility that wave activity was prevalent earlier in the evolution of the structure which was responsible for isotropizing the electron distribution. It is also possible that there could be electromagnetic waves at lower frequencies (e.g., whistler modes) which are out of the range of the instrument; the very high β inside the depressions (see Figure 3) would favor the operation of electromagnetic instabilities which might be responsible for scattering. The observations of reduced plasma wave activity within the depressions contrast with the observations of *Lin et al.* [1995] which suggest that Langmuir waves are enhanced during magnetic holes.

5. Structure of the Depression Boundaries

Both of the magnetic depressions are bounded at each edge by sharp discontinuities. We have used two methods to estimate the normal directions to the planes of the discontinuities. Firstly, a variance analysis [*Sonnerup and Cahill*, 1967] was performed on each boundary for the high-resolution (0.125 s sampling) and 5 s magnetic field data from AMPTE UKS, 5 s data from AMPTE IRM, and 4 s data from ISEE 1; the estimated normals to the discontinuities are given by the minimum variance directions. Secondly, the normal direction was computed from the vector cross product between the average preboundary and postboundary magnetic field directions. This method assumes that the boundaries are planar tangential discontinuities, which the results detailed below confirm. Figure 6 presents the leading edge of the second depression as observed in the AMPTE UKS high-resolution data and shows the variance analysis which suggests that this is a tangential discontinuity. The boundary is ~750 km thick (~2 s transition with V_{sw} ~375 km s^{-1}), which represents a spatial extent ~5-10 R_L (ion Larmor radii).

The results of the boundary orientation analysis described above for all the boundaries are presented in Figure 7 as a direction in GSE colatitude θ_{GSE} and GSE longitude ϕ_{GSE}. The orientation of the normals has a 180° ambiguity, and so those presented here represent

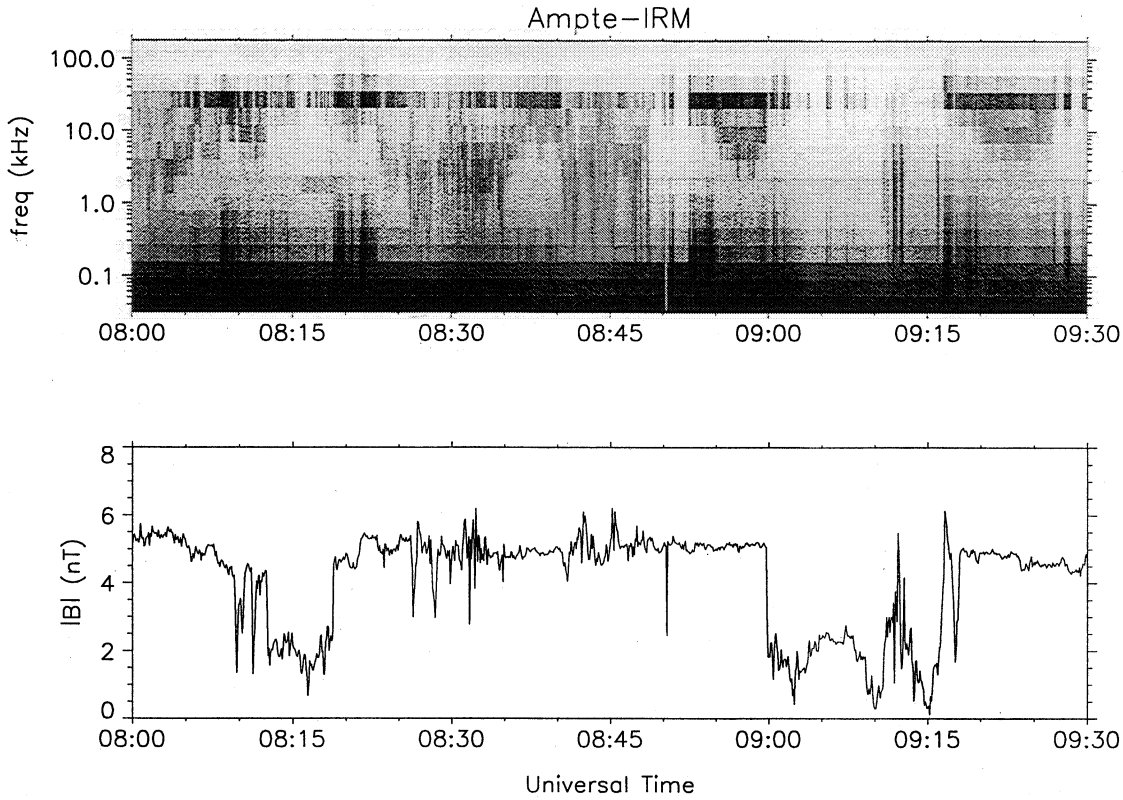

Figure 5. (top) Plasma wave data from the AMPTE IRM ELF/MF spectrum analyzer for the interval 0800 - 0930 UT. (bottom) Magnetic field magnitude measured by AMPTE IRM for the same interval.

the normals pointing away from the structures. The ratio of the intermediate to minimum variance eigenvalues (λ_2/λ_3) was greater than 7 for all the estimates shown, which suggests that the structure boundaries are essentially planar and that the normals are well defined. Changing the precise intervals over which the minimum variance and cross-product normal evaluations were performed had little effect on the normal directions estimated, which further enforces their reliability.

In Figure 7 the estimates clustered around $\phi_{GSE} = 180°$ represent the leading edges of the depressions whereas those clustered around $\phi_{GSE} = 0°$ represent the trailing edges of the depressions. The normal estimates for each boundary are generally consistent regardless of the spacecraft, data type, or analysis method used. However, the trailing edge of the second depression shows more variability, especially with the estimates made using the cross-product method. This is most likely a consequence of contamination by backstreaming ions from the bow shock. The velocity spike evident in Figure 3 at this time would tend to support this interpretation. The results presented in Figure 7 show that the depression boundaries are roughly perpendicular to the GSE x axis, being inclined by ~20° with respect to the GSE y-z plane. The ambient IMF direction at this time is almost strictly in the negative GSE y direction.

The estimations of the boundary normal directions can be used to determine whether they are tangential or rotational discontinuities. Tangential discontinuities would suggest that the depressions are magnetically separate structures. Perfect tangential discontinuities have $B_n = 0$, where B_n is the normal component of the magnetic field. In practice, owing to errors in determining the normal and nonplanar effects, tangential discontinuities are identified by a relatively small B_n compared to the total field strength $|B|$. By contrast, rotational discontinuities have a finite B_n which can be comparable to $|B|$ and have no change in field magnitude ($\Delta|B| = 0$). Figure 8 shows a test of these two criteria for all the depression edges observed by all the spacecraft. In all cases, $B_n/|B| < 0.4$ and $\Delta|B|/|B| > 0.2$, implying that all the depression boundaries represent tangential discontinuities.

We can use the estimated normals and the multispacecraft observations to show that the structures are convecting with the solar wind. The second of the two depressions was observed by ISEE 1 located upstream of AMPTE UKS and IRM (see Figure 1). A delay of ~119±5 s occurred between the boundaries of the depression as observed by ISEE 1 and AMPTE UKS. The expected time delay, assuming convection with the solar wind, can be evaluated using

$$\Delta t = \frac{\mathbf{\Delta x} \cdot \hat{\mathbf{n}}}{\mathbf{V}_{flow} \cdot \hat{\mathbf{n}}}, \quad (1)$$

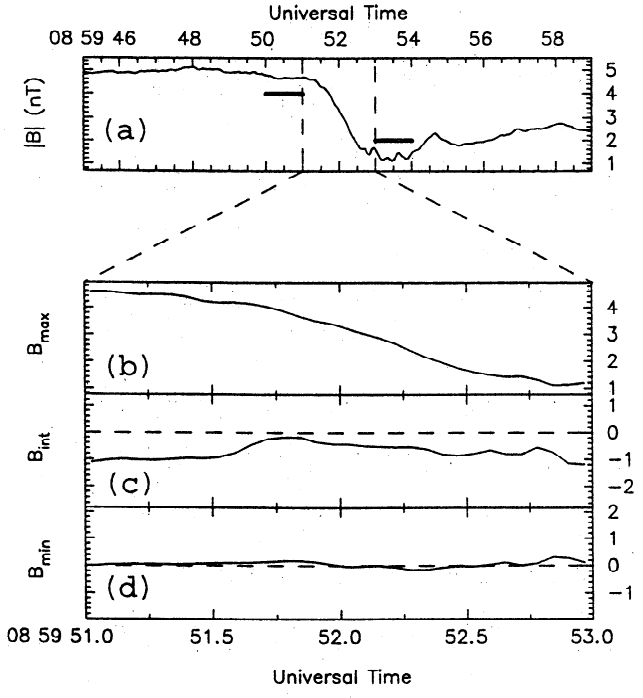

Figure 6. (a) The high-resolution magnetic field magnitude from AMPTE UKS for the leading edge of the second depression. The dashed lines represent the extent of the time period employed in the variance analysis in this case. (b-d) Expanded time interval from Figure 6a showing the magnetic field variation in the maximum, intermediate and minimum variance directions. The bold lines in Figure 6a represent the preboundary and postboundary time intervals used in the cross-product analysis in this case.

where $\mathbf{\Delta x}$ represents the spacecraft separation vector, $\mathbf{V}_{flow}$ is the solar wind flow velocity, and $\hat{\mathbf{n}}$ represents the normal to the depression boundary. The spacecraft separation vector $\mathbf{\Delta x} = \mathbf{x}_{UKS} - \mathbf{x}_{ISEE}$ at ~0900 UT is (-6.77, 1.63, 1.92) R_E (GSE), the solar wind flow velocity as measured by AMPTE UKS is (-377, 17, -4) km s^{-1} (GSE), and the average boundary normal direction from the AMPTE UKS and ISEE 1 minimum variance analysis is (0.964, 0.201, -0.173) (GSE). Entering these values into (1) results in a Δt of 116±9 s, which is within the error of the observed delay and confirms that the structure is convecting with the solar wind.

6. Evolution of the Depression Magnetic Field

The location of ISEE 1, ~6 R_E farther upstream from AMPTE UKS and IRM, allows us to study the internal magnetic field structure of the depressions as they convect with the solar wind and to determine whether they appear to be static or evolving structures. Figure 9 presents the IMF variations observed by ISEE 1 and AMPTE UKS for an interval containing the second depression. Figures 9a–9c represent the IMF magnitude ($|B|$) and the IMF orientation in GSE colatitude (θ_B), and GSE longitude (ϕ_B), respectively. The bold lines represent the AMPTE UKS variations, and the dotted lines represent the ISEE 1 variations shifted by 119 s as suggested by the time delay measured in section 5. The vertical dashed lines delineate the interval when AMPTE UKS was located within the ion foreshock.

It is clear from Figure 9 that directly before and after the depression the IMF magnitude and direction observed at both the spacecraft are almost identical. However, within the depression there are some differences between the two spacecraft observations, especially concerning the IMF direction. The interval between the dashed lines should be excluded from this discussion as during this interval the magnetic field at AMPTE UKS will be affected by back-streaming ions from the bow shock. Early in the depression there are intervals where the IMF direction differs by large amounts between the two spacecraft. A maximum difference of ~100° occurs in θ_B, and a maximum difference of ~170° occurs in ϕ_B. However, the overall gross variations are very similar. These differences are probably a result of the spatial structure of the depression; the two spacecraft are sep-

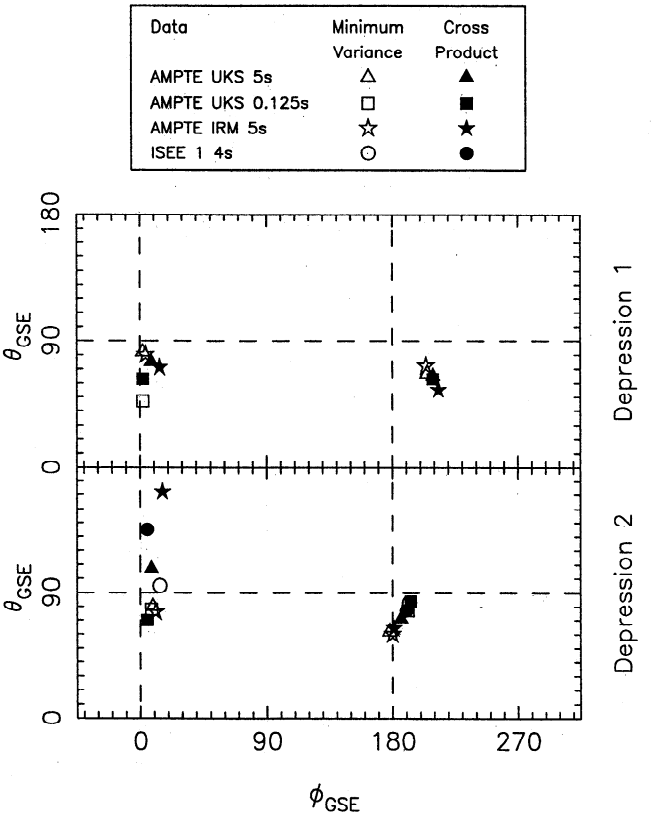

Figure 7. Normals to the depression boundaries estimated using the minimum variance technique (open symbols) and the vector cross product (solid symbols). The normals for the two depressions are shown separately and represent the boundary normals pointing away from the depression. The normals clustered around $\phi = 180°$ represent the leading edge normals whereas those clustered around $\phi = 0°$ represent the trailing edge normals.

arated by ~1-2 R_E in the GSE y direction. However, it is also possible that the differences observed show evidence that the internal structure of the depression is evolving as it convects with the ambient solar wind.

7. Discussion

There are two very different interpretations which could explain the observations presented, and we shall attempt to discriminate between the two. Firstly, the observations could represent brief encounters with the HPS which do not involve a complete crossing of the HCS but instead show a retreat back to the original IMF sector. Secondly, the observations could describe magnetic holes created by the mirror instability in a later stage of their evolution than is generally observed.

There are features of the depressions which might suggest a HPS encounter: a reduction in $|B|$, enhanced plasma density n, and enhanced plasma β. The feature most suggestive of an encounter with the HPS/HCS is the magnetic field reversal observed between 0908 and 0911 UT by AMPTE UKS (see Figure 9; the timing and structure are slightly different at ISEE 1). This time is also characterized by the lowest magnetic field intensity during the depression. The reversal appears short-lived; there is no overall IMF reversal across the whole depression. However, it could be possible that it represents a brief encounter with the HCS.

Using solar observations, we have tried to determine whether our observations are in close proximity to the HCS. Photospheric and coronal synoptic maps show that the solar field is very complex during this Carrington rotation (not shown), with large equatorial islands of antisunward polarity embedded in sunward regions at coronal heights, mapping to isolated sunward regions embedded in large antisunward regions at photospheric heights. Only at heliolatitudes above 45° does the solar dipole show any systematic behavior. We have also studied the IMF polarity during this interval as observed by ISEE 1 in the IMF. The ISEE 1 data show a sector boundary crossing close to 0300 UT on November 27, 1984, as well as a possible brief encounter with the HCS late on November 25, 1984, with the spacecraft returning to the original IMF sector. Although the interval containing the depressions is in a unipolarity IMF region, the complexity of the solar magnetic field at this time does not rule out an encounter with the HPS/HCS.

If it is that our two depressions do represent penetration of the HPS, then since our observations do

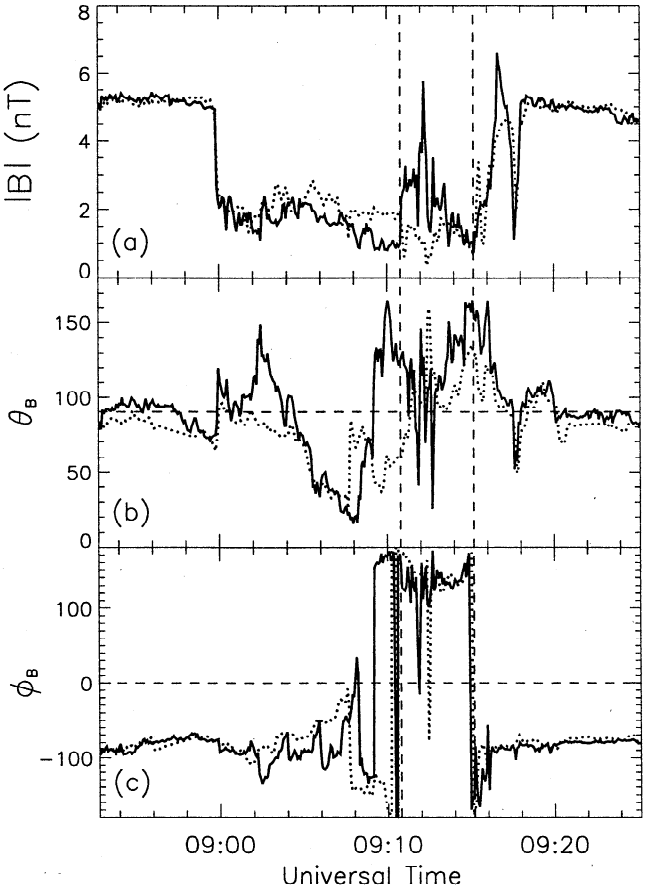

Figure 9. Plots of the interplanetary magnetic field (IMF) variations during the second depression as observed by AMPTE UKS (bold lines) and ISEE 1 (dotted lines): (a) The IMF magnitude ($|B|$), (b) the IMF orientation in GSE colatitude (θ_B), and (c) the IMF orientation in GSE longitude (ϕ_B). The ISEE 1 data have been shifted by 119 s to account for the convection with the solar wind. The vertical dashed lines delineate the interval where AMPTE UKS was located within the ion foreshock.

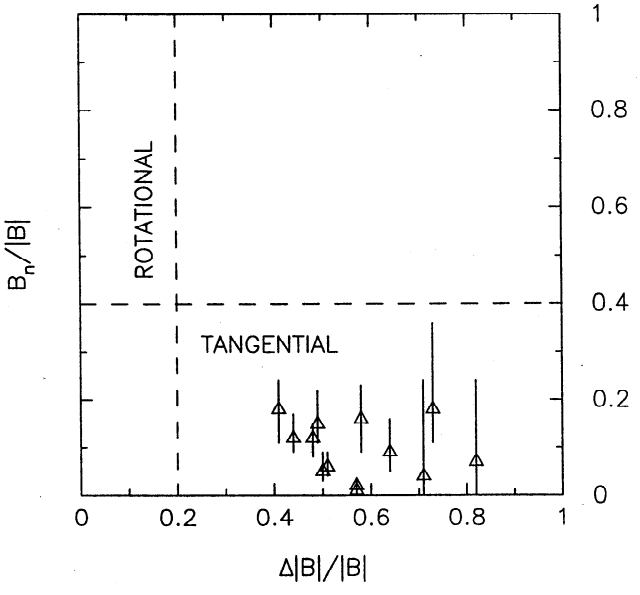

Figure 8. Plot of $B_n/|B|$ against $\Delta|B|/|B|$ for the boundary discontinuities as measured on all the spacecraft, showing that all the boundaries represent tangential discontinuities. The dashed lines represent the limits to the thresholds suggested by *Neugebauer et al.* [1984] to identify rotational verses tangential discontinuities.

not show a complete HCS crossing, we must be observing the passage through a rippled, wavelike HPS boundary. Some previous observations have suggested that the HCS has a rippled appearance [e.g., *Behannon et al.*, 1981] with surface variations with wavelengths ~0.05 - 0.1 AU superimposed on the larger-scale structure. If this is the case for these observations, the HPS boundary would need to be severely warped; both depression boundaries are aligned very close to the GSE y-z plane. Taking the two boundary normals for the second depression suggests a radius of curvature for the structure ~60 R_E; the average HPS thickness is ~50 R_E [*Winterhalter et al.*, 1994a], which would suggest that the HPS is severely kinked on a very small scale. The observed depression boundaries are sharp tangential discontinuities. Previous observations of the HPS boundary [e.g., *Winterhalter et al.*, 1994a] show no evidence of either a sharp tangential discontinuity or a severely rippled boundary with variations at such small scale lengths.

Before the start of the first depression at ~0813 UT, the two AMPTE spacecraft also observe two shorter reductions in the magnetic field intensity at ~0810 and ~0811 UT (see Figure 3). These dips last for ~20 s and as with the larger depressions are bounded by tangential discontinuities with normals oriented approximately in the GSE x direction. These dips show very little change in IMF direction (~30°) and have all the characteristics of previously observed "linear" magnetic holes [e.g., *Winterhalter et al.*, 1994b]. These small dips seem extremely unlikely to be observations of the rippled surface of the HPS boundary and appear to further argue against the HPS encounter hypothesis. If these observations did indeed represent an encounter with the HPS, then they would describe large-amplitude, small-wavelength variations of the HPS boundary, which would be unique to the literature.

There is still the observed dropout in the electron heat flux that could suggest a link with HFDs which are generally associated with the HPS. However, the depressions do not display all the typical characteristics of HFDs such as reductions in bulk velocity and temperature. HFDs are often thought to be detached magnetic structures. However, the depressions do not display bidirectional halo electron signatures, which are characteristic of detached magnetic structures. This appears to argue against any association between the depressions and HFDs.

Next we consider whether the depressions represent magnetic holes, created by the mirror instability, in a more evolved state than has generally been observed. If this is the case, then these depressions would most likely represent a conglomeration of a number of closely spaced holes. The observation of two typical "linear" magnetic holes immediately before the first depression appears to support this interpretation. It has been previously suggested [e.g., *Winterhalter et al.*, 1994b] that magnetic holes may be the remnants of mirror mode structures created upstream of their point of observation. Because of the large value of β (~10) inside the depressions (see Figure 3), only a small ion temperature anisotropy, $T_\perp/T_\parallel > 1.1$ (not available for present study), would render the plasma inside the depressions mirror unstable. However, it is likely that these depressions have attained marginal stability. The reduction in plasma wave activity within the holes does not fit with previous magnetic hole observations, although it could be that plasma waves are only characteristic of magnetic holes which are still mirror unstable.

8. Summary

It is difficult to be entirely clear on the origins of the large magnetic depressions described in this paper. They do not show the large number of directional discontinuities associated with PMSs or the anomalous flow characteristics of the bow shock associated HFAs and so are not related to these phenomena. There are features which suggest that the depressions represent an encounter with the HPS, although no complete magnetic field reversal which would indicate a crossing of the HCS is observed, and the HPS would need to have an abnormally kinked surface with unusually steep tangential discontinuity boundaries for this to be the case. For this reason, it seems more likely that these events represent a large magnetic hole caused by a conglomeration of smaller holes which have grown out of the mirror instability. The observations of two typical "linear" magnetic holes before the first depression appear to support this interpretation. If this is the case, then these represent unique observations of large magnetic holes; these larger holes have probably been missed in previous magnetic hole studies owing to the selection criteria employed. However, there are several features of these depressions, such as the variation of the magnetic field structure within them and the dropout in the electron heat flux, which are not fully explained by present theories of magnetic holes.

Acknowledgments. The AMPTE UKS electron data were kindly provided by Mike Hapgood at DRAL, and the ion data were supplied by MSSL, U.K., P.I. Alan Johnstone. The AMPTE IRM wave data are part of the IRM PDB data set, P.I. Rudolf Treumann, MPE, Garching, Germany. We would like to thank the referees for useful comments. We would also like to acknowledge support from grants from the U.K. Particle Physics and Astronomy Research Council.

Michel Blanc thanks Michelle Thomsen and Daniel Winterhalter for their assistance in evaluating this paper.

References

Behannon, K.W., F.M. Neubauer, and H. Barnstorf, Fine-scale characteristics of interplanetary sector boundaries, *J. Geophys. Res., 86*, 3273, 1981.

Burlaga, L.F., Micro-scale structures in the interplanetary medium, *Sol. Phys., 4*, 67, 1968.

Chisham, G., S.J. Schwartz, and D. Burgess, The anisotropy variations of electron distributions in the terrestrial ion foreshock, *J. Geophys. Res., 101*, 445, 1996.

Chisham, G., S.D. Bale, D. Burgess, and S.J. Schwartz, A large magnetic depression observed in the solar wind close to the Earth's bow shock, *Adv. Space Res., 19*(6), 869, 1997.

Coates, A.J., J.A. Bowles, R.A. Gowen, B.K. Hancock, A.D. Johnstone, and S.J. Kellock, The AMPTE UKS three-dimensional ion experiment, *IEEE Trans. Geosci. Remote Sens., 23*, 287, 1985.

Crooker, N.U., M.E. Burton, J.L. Phillips, E.J. Smith, and A. Balogh, Heliospheric plasma sheets as small-scale transients, *J. Geophys. Res., 101*, 2467, 1996a.

Crooker, N.U., M.E. Burton, G.L. Siscoe, S.W. Kahler, J.T. Gosling, and E.J. Smith, Solar-wind streamer belt structure, *J. Geophys. Res., 101*, 24,331, 1996b.

Dobrowolny, M., B. Bavassano, F. Mariani, and N. Ness, Magnetic dips in the solar wind, *Sol. Phys., 62*, 203, 1979.

Farrugia, C.J., M.W. Dunlop, F. Guerts, A. Balogh, D.J. Southwood, D.A. Bryant, M. Neugebauer, and A. Etemadi, An interplanetary planar magnetic structure oriented at a large (approximately 80 deg) angle to the parker spiral, *Geophys. Res. Lett., 17*, 1025, 1990.

Fitzenreiter, R.J., and K.W. Ogilvie, Heat flux dropouts in the solar wind and Coulomb scattering effects, *J. Geophys. Res., 97*, 19,213, 1992.

Gurnett, D.A., Plasma waves and instabilities, in *Collisionless Shocks in the Heliosphere: Reviews of Current Research, Geophys. Monogr. Ser.*, vol. 35, edited by B.T. Tsurutani and R.G. Stone, pp. 207–224, AGU, Washington, D.C., 1985.

Häusler, B., et al., The plasma wave instrument on board the AMPTE IRM satellite, *IEEE Trans. Geosci. Remote Sens., GE-23*, 267, 1985.

Klein, L., and L.F. Burlaga, Interplanetary sector boundaries 1971-1973, *J. Geophys. Res., 85*, 2269, 1980.

Lin, N.G., P.J. Kellogg, R.J. MacDowall, A. Balogh, R.J. Forsyth, J.L. Phillips, A. Buttighoffer, and M. Pick, Observations of plasma-waves in magnetic holes, *Geophys. Res. Lett., 22*, 3417, 1995.

Lühr, H., N. Klöcker, W. Oelschlägel, B. Häusler, and M. Acuña, The IRM fluxgate magnetometer, *IEEE Trans. Geosci. Remote Sens., GE-23*, 259, 1985.

MacDowall, R.J., N. Lin, P.J. Kellogg, A. Balogh, R.J. Forsyth, and M. Neugebauer, Langmuir waves in magnetic holes: Source mechanism and consequences, *Proceedings of the Eighth International Solar Wind Conference*, edited by D. Winterhalter et al., pp. 301–304, Am. Inst. of Phys., Woodbury, New York, 1996.

McComas, D.J., J.T. Gosling, J.L. Phillips, S.J. Bame, J.G. Luhmann, and E.J. Smith, Electron heat flux dropouts in the solar wind: Evidence for interplanetary magnetic field reconnection?, *J. Geophys. Res., 94*, 6907, 1989.

Nakagawa, T., A. Nishida, and T. Saito, Planar magnetic structures in the solar wind, *J. Geophys. Res., 94*, 11,761, 1989.

Neugebauer, M., D.R. Clay, B.E. Goldstein, B.T. Tsurutani, and R.D. Zwickl, A reexamination of rotational and tangential discontinuities in the solar wind, *J. Geophys. Res., 89*, 5395, 1984.

Pantellini, F.G.E., A model of the formation of stable non-propagating magnetic structures in the solar wind based on the nonlinear mirror instability, *J. Geophys. Res., 103*, 4789, 1998.

Phillips, J.L., J.T. Gosling, D.J. McComas, S.J. Bame, S.P. Gary, and E.J. Smith, Anisotropic thermal electron distributions in the solar wind, *J. Geophys. Res., 94*, 6563, 1989.

Russell, C.T., The ISEE 1 and 2 fluxgate magnetometers, *IEEE Trans. Geosci. Electron., GE-16*, 239, 1978.

Schwartz, S.J., Hot flow anomalies near the Earth's bow shock, *Adv. Space Res., 15*(8/9), 107, 1995.

Schwartz, S.J., et al., An active current sheet in the solar wind, *Nature, 318*, 269, 1985.

Shah, H.M., D.S. Hall, and C.P. Chaloner, The electron experiment on AMPTE UKS, *IEEE Trans. Geosci. Remote Sens., GE-23*, 293, 1985.

Sonnerup, B.U.O., and L.J. Cahill Jr., Magnetopause structure and attitude from Explorer 12 observations, *J. Geophys. Res., 72*, 171, 1967.

Southwood, D.J., W.A.C. Mier-Jedrzejowicz, and C.T. Russell, The fluxgate magnetometer for the AMPTE UK Subsatellite, *IEEE Trans. Geosci. Remote Sens., GE-23*, 301, 1985.

Thomsen, M.F., J.T. Gosling, S.A. Fuselier, S.J. Bame, and C.T. Russell, Hot diamagnetic cavities upstream from the Earth's bow shock, *J. Geophys. Res., 91*, 2961, 1986.

Tsurutani, B.T., E.J. Smith, D.J. Southwood, and A. Balogh, Nonlinear magnetosonic waves and mirror mode structures in the March 1991 Ulysses interplanetary event, *Geophys. Res. Lett., 19*, 1267, 1992.

Turner, J.M., L.F. Burlaga, N.F. Ness, and J.F. Lemaire, Magnetic holes in the solar wind, *J. Geophys. Res., 82*, 1921, 1977.

Winterhalter, D., E.J. Smith, M.E. Burton, N. Murphy, and D.J. McComas, The heliospheric plasma sheet, *J. Geophys. Res., 99*, 6667, 1994a.

Winterhalter, D., M. Neugebauer, B.E. Goldstein, E.J. Smith, S.J. Bame, and A. Balogh, Ulysses field and plasma observations of magnetic holes in the solar wind and their relation to mirror-mode structures, *J. Geophys. Res., 99*, 23,371, 1994b.

S. D. Bale, Space Sciences Laboratory, Centennial Drive at Grizzly Peak Boulevard, University of California, Berkeley, CA 94720-7450. (bale@ssl.berkeley.edu)

D. Burgess and S. J. Schwartz, Astronomy Unit, Queen Mary and Westfield College, Mile End Road, London E1 4NS, England, U.K. (D.Burgess@qmw.ac.uk; S.J.Schwartz@qmw.ac.uk)

G. Chisham, British Antarctic Survey, Natural Environment Research Council, High Cross, Madingley Road, Cambridge CB3 0ET, England, U.K. (G.Chisham@bas.ac.uk)

M. W. Dunlop, Space and Atmospheric Physics Group, Imperial College of Science, Technology and Medicine, London SW7 2BZ, England, U.K. (m.dunlop@ic.ac.uk)

C. T. Russell, Institute of Geophysics and Planetary Physics, University of California, Los Angeles, CA 90095-1567. (ctrussel@igpp.ucla.edu)

(Received January 15, 1999; revised June 15, 1999; accepted September 6, 1999.)